The Journal of Experimental Biology 215, 3631-3638

doi:10.1242/jeb.073627

RESEARCH ARTICLE

Neuromuscular and biomechanical compensation for wing asymmetry in insect hovering flight

María José Fernández[1,*], Dwight Springthorpe[2] and Tyson L. Hedrick[1]

[1]Department of Biology, University of North Carolina, Chapel Hill, NC 27599, USA and [2]Department of Integrative Biology, University of California, Berkeley, CA 94720, USA

*Corresponding author at present address: Faculty of Biological Sciences, University of Leeds, Leeds LS2 9JT, UK (m.j.fernandez@leeds.ac.uk)

SUMMARY

Wing damage is common in flying insects and has been studied using a variety of approaches to assess its biomechanical and fitness consequences. Results of these studies range from strong to nil effect among the variety of species, fitness measurements and damage modes studied, suggesting that not all damage modes are equal and that insects may be well adapted to compensate for some types of damage. Here, we examine the biomechanical and neuromuscular means by which flying insects compensate for asymmetric wing damage, which is expected to produce asymmetric flight forces and torques and thus destabilize the animal in addition to reducing its total wing size. We measured the kinematic and neuromuscular responses of hawkmoths (*Manduca sexta*) hovering in free flight with asymmetrically damaged wings *via* high-speed videography and extracellular neuromuscular activity recordings. The animals responded to asymmetric wing damage with asymmetric changes to wing stroke amplitude sufficient to restore symmetry in lift production. These asymmetries in stroke amplitude were significantly correlated with bilateral asymmetries in the timing of activation of the dorsal ventral muscle among and within trials. Correspondingly, the magnitude of wing asymmetry was significantly, although non-linearly, correlated with the magnitude of the neuromuscular response among individuals. The strongly non-linear nature of the relationship suggests that active neural compensation for asymmetric wing damage may only be necessary above a threshold (>12% asymmetry in wing second moment of area in this case) below which passive mechanisms may be adequate to maintain flight stability.

Supplementary material available online at http://jeb.biologists.org/cgi/content/full/215/20/3631/DC1

Key words: electromyography, *Manduca sexta*, wingbeat kinematics, stability.

Received 11 April 2012; Accepted 29 June 2012

INTRODUCTION

Flight performance is crucial to the fitness of many flying organisms. During flight, animals often suffer wing damage due to predation (Robbins, 1981; Rodd et al., 1980), competition (Alcock, 1996) or accidental collisions with their environment (Foster and Cartar, 2011a; Higginson and Barnard, 2004; Higginson and Gilbert, 2004; Wootton, 1992). Studies in birds (Swaddle, 1997; Swaddle and Witter, 1998), dragonflies (Combes et al., 2010) and tethered midges (McLachlan, 1997) have shown that natural and artificial wing damage decreases various aspects of flight performance, consequently decreasing broader measures of fitness (Cartar, 1992; Combes et al., 2010). However, Hedenström et al. (Hedenström et al., 2001) found no effect on flight performance following wing damage on bumblebees. Furthermore, studies on butterflies (Kingsolver, 1999) and bumblebees (Haas and Cartar, 2008) found that individuals with damaged wings had fitness similar to that of individuals without damaged wings. These disparate results suggest that not all types of damage are equal and that animals may be adept at compensating for some forms of wing damage.

In most of the aforementioned studies, wing wear or damage was applied symmetrically to isolate the effects of wing shape and size on flight performance. However, natural damage may occur asymmetrically. In this case, if the damaged animal maintains symmetric wing kinematics, asymmetric aerodynamic forces and torques will result, potentially destabilizing flight. Thus, animals with asymmetric wing shapes must use asymmetric wing kinematics to produce symmetric forces and torques, potentially increasing the difficulty of compensation for wing damage. Nevertheless, animals with damaged, asymmetric wings are able to maintain flight stability and perform complex manoeuvres (Haas and Cartar, 2008). Here we investigate the biomechanical and neuromuscular means by which flying animals compensate for asymmetrically damaged wings and maintain flight stability, building on prior investigation of the causes and effects of wing damage (Foster and Cartar, 2011a; Foster and Cartar, 2011b; Hedenström et al., 2001; Higginson and Barnard, 2004; Rodd et al., 1980).

Organisms maintain locomotor stability with active neural mechanisms, passive non-neural mechanisms or a combination of the two (Dickinson et al., 2000; Nishikawa et al., 2007). The relative importance of these sources of stability may depend on the speed of locomotion and magnitude of perturbation. For example, studies in fast terrestrial locomotion such as running show that organisms are able to overcome perturbations with minimal neural input through the intrinsic biomechanical properties of their legs (Daley and Biewener, 2006; Daley et al., 2009; Jindrich and Full, 2002; Sponberg and Full, 2008). Because the passive stability mechanisms revealed in these studies are not subject to synaptic or muscle activation delays, they likely offer an advantage to the organism, allowing it to respond more quickly to a perturbation compared with active neural responses (Daley et al., 2009; Jindrich and Full, 2002;

Revzen, 2009). Passive stability mechanisms are also found in flapping flight (Hedrick et al., 2009), where they play a role in the recovery reactions of fruit flies following in-flight perturbation (Ristroph et al., 2010) and may also help maintain stability following asymmetric wing damage.

Organisms that suffer large perturbations require neural feedback to actively stabilize their locomotion in addition to passive stability mechanisms (Sponberg and Full, 2008). Organisms also use active neural modulation to perform voluntary manoeuvres (Büschges, 2005; Cruse, 1990; Cruse et al., 2007) and after perturbations during slow locomotion, such as walking (Dietz et al., 1987; Gorassini et al., 1994; Marigold and Patla, 2005). The slower nature of these behaviours may make the latencies associated with active neural mechanisms less problematic than during fast locomotion, where active response latencies might approach the duration of a single locomotor cycle such as a stride. Similarly, voluntary manoeuvres in aerial locomotion (Kammer, 1971; Springthorpe et al., 2012; Sponberg and Daniel, 2012; Wang et al., 2008) require neural modulation, which may be used to produce a counter manoeuvre following perturbation. Recently, Cheng et al. (Cheng et al., 2011) showed that hawkmoths use both passive and active mechanisms during an avoidance response to a visual stimulus. In this case, moths use passive damping to reduce body translational and angular velocity, but use an active mechanism to control their orientation.

Compensation for asymmetric wings may thus incorporate one or both of passive non-neural mechanisms and active neural responses. Given the advantages these passive, non-neural mechanisms bring through reduction in the latency of response, we hypothesize that flying animals have evolved to use these mechanisms to compensate for wing damage and other in-flight perturbations. We specifically propose that flying insects compensate for asymmetric wings *via* the following passive mechanism: because the damaged wing has reduced area, it produces lower aerodynamic forces and torques compared with the intact wing, given the same wing motion. However, if the flight muscles of this damaged wing apply the same force or torque to it as was applied to the original, undamaged wing, the wing will speed up, increasing the aerodynamic torque produced by that wing until the muscle and aerodynamic torques are equal and the wing ceases accelerating. In short, the mismatch between muscle and wing following wing damage could lead to additional wing acceleration and greater velocity. Consequently, we expect that the damaged wing will have greater stroke amplitude than the intact wing, because the damaged wing's greater angular velocity will cause it to cover a larger arc in the same time interval. Moreover, these changes in kinematics will not have a corresponding asymmetry in the neural activation of the wing muscles and we therefore refer to them as a passive stability mechanism because they arise due to the fundamental force–velocity properties of muscle and not a sensor-based feedback loop.

In keeping with the hypothesized muscle-based passive stability mechanism for flapping flight, we predict that a simple aerodynamic analysis based on wing morphology, flapping amplitude and flapping frequency will show that the asymmetric flapping kinematics adopted by moths with damaged wings lead to equal aerodynamic torque on both wings. Crucially, we also expect that because these changes in kinematics arise from intrinsic muscle properties and wing aerodynamics, they will not involve neuromuscular asymmetries. If our hypothesis is false, we will instead observe asymmetries in wingbeat kinematics coupled with neuromuscular asymmetries; this would indicate that neural modulation contributes to stabilization in flapping with asymmetric wings. Here, we test these hypotheses by simultaneously recording wingbeat kinematics and flight muscle electromyograms (EMGs), from which we extract activation phases, from hovering, freely flying tobacco hornworm moths (*Manduca sexta*) with both symmetric and asymmetric artificially reduced wings.

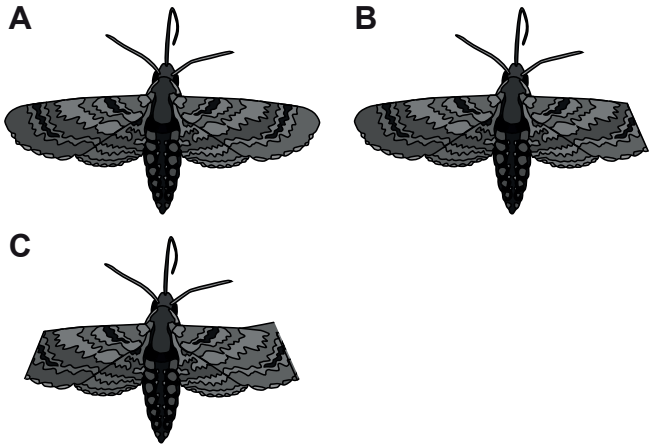

Fig. 1. Schematic representation of the treatments applied to each individual moth. (A) Control or fully intact wings. (B) Asymmetric wing clipping, where the moth has only one forewing tip clipped. (C) Symmetric wing clipping, where both forewings have been clipped.

MATERIALS AND METHODS

Animals

We obtained male *Manduca sexta* (Linnaeus 1763) pupae from the Department of Biology at Duke University. Pupae and adult moths were housed in fabric mesh cages (30×30×30 cm) at 25±3°C. We maintained pupae under a 20 h:4 h light:dark photoperiod while we kept adult moths under a 22 h:2 h light:dark cycle to minimize activity and avoid additional wing damage during caged flight. We fed the moths daily with an artificial nectar solution (1:4 honey:water) to maintain their body mass. To elicit stable hovering and feeding behaviour, we presented the adult moths with natural and artificial flowers on the second day following eclosion. We reinforced this behaviour daily with a food reward until the moth showed interest in feeding immediately after flower presentation. Moths became experimental candidates only after reliably demonstrating prolonged stationary hovering and feeding behaviour.

Experimental design

We measured muscle activity and obtained video recordings for kinematic analyses while moths hovered in front of an artificial flower inside a large glass chamber (0.7×0.7×0.7 m) illuminated with eight infrared (760 nm) lights (Roithner LaserTechnik, Vienna, Austria). Each moth was exposed to three experimental conditions (Fig. 1): (1) fully intact wings (control), (2) asymmetric wing clipping (one forewing clipped; side randomly chosen) and (3) approximately symmetric wing clipping (both forewings similarly clipped). Treatments were applied in order. In clipping a wing, we removed between 5 and 18% of the area of a single wing, which corresponded to a 13–27% decrease in length, a 18–40% decrease in second moment of area, and a 24–51% decrease in third moment of area (see Table 1). We recorded body mass at the end of each of the three experimental conditions using an electronic balance (±0.0001 g; Adventurer Pro, Ohaus Corporation, Pine Brook, NJ, USA).

Table 1. Morphological parameters for individual moths' wings during intact and clipped wing treatments

		Wing area (cm^2)		Length (cm)		Second moment (cm^4)		Third moment (cm^5)	
Moth	Treatment	L	R	L	R	L	R	L	R
1	Intact	9.53	9.26	4.89	4.83	64.93	55.93	218.74	182.84
1	Clipped	7.78	7.99	3.57	3.73	39.13	35.39	106.89	94.72
2	Intact	9.61	9.24	4.67	4.56	60.70	53.89	198.69	169.85
2	Clipped	8.39	8.23	3.73	3.72	38.40	39.54	105.56	110.15
3	Intact	10.6	9.90	4.77	4.69	66.28	61.70	218.50	200.75
3	Clipped	9.61	9.11	4.05	4.03	49.99	50.84	147.84	151.95
4	Intact	10.22	10.16	4.65	4.82	68.12	68.13	223.01	226.62
4	Clipped	9.29	9.00	4.03	3.87	50.69	47.74	148.31	137.89
5	Intact	9.96	9.27	4.97	4.71	66.07	54.81	222.97	172.12
5	Clipped	8.74	8.31	3.70	3.72	40.05	37.19	110.88	99.67

Asymmetric trials were recorded from moths 1, 2 and 4 after clipping the left (L) wing and in moths 3 and 5 after clipping the right (R) wing.
Data used in this table are available in supplementary material Table S1.

Electrode implantation and EMGs

We implanted electrodes and made EMG recordings as described previously (Springthorpe et al., 2012). Briefly, we cooled each moth for 5 to 10 min at 5°C to reduce agitation before electrode implantation. Once the moth became quiescent, we secured it to a chilled operating table using padded clamps over its wings. We implanted single electrodes in four different muscles (Fig. 2A): the left and right dorsal longitudinal muscles (DLMs; which power the downstroke), and the left and right dorsal ventral muscles (DVMs; which power the upstroke; Pringle, 1957). Electrodes consisted of a 1–2 mm long and 0.1 mm diameter tungsten wire (A-M Systems, Carlsborg, WA, USA), electrically and physically bonded to a 1 m long copper signal wire (0.15 mm diameter, enamel coated, EIS/Fay Electric Wire, Elmhurst, IL, USA). We secured the electrodes to the animal at the insertion site and also at the tip of the abdomen using cyanoacrylate adhesive (Loctite Super Glue, Henkel, Avon, OH, USA). After implantation, we allowed the moths to rest for at least 1 h and until they demonstrated normal flight behaviour. Implanted moths that did not resume typical flight behaviour were discarded from further analysis.

We connected ipsilateral electrodes (e.g. left DLM and left DVM) to a differential amplifier (gain: 100×, analogue filters: 10 Hz–10 kHz bandpass, 60 Hz notch; Model 1800, A-M Systems; see Fig. 2A). A data acquisition system (USB-6251, National Instruments, Austin, TX, USA), controlled by MATLAB (The MathWorks, Natick, MA), saved the signal from the amplifier. Although this electrode implant scheme minimizes the number of electrodes required, it places the signals from both the DLM and DVM muscles from one side of the animal on a single amplifier channel. To differentiate the DLM and DVM signals, we compared EMG signals with the corresponding video recordings (see below).

We processed the EMG data to extract the activation phase relative to the wingbeat cycle. Activation phase has been correlated with wing kinematic changes in hawkmoths (Kammer, 1971; Rheuben and Kammer, 1987), and expression of activation timing in terms of wingbeat phase automatically normalizes muscle activity with regard to wingbeat frequency. We first applied a bandpass, fourth-order Butterworth filter (200–600 Hz) to each signal, and then we extracted the raw activation times (t_{muscle}) and converted them into left–right phase differences (for the two symmetric treatments; control and both wings clipped) and clipped–unclipped difference (for the asymmetry treatment), relative to a wingbeat period. We have defined the wingbeat period here as the time between two subsequent DLM activation events (averaged between left and right sides; see Fig. 2B). Because of the DLM regularity and bilateral symmetry, it is usually used as the reference muscle for each wingbeat (Kammer, 1971; Wang et al., 2008). We calculated the activation phase difference ($\Delta\phi_{muscle}$) of each muscle relative to the wingbeat, normalizing the data (Kammer, 1971; Rheuben and Kammer, 1987) from the processed EMG signal on both sides. For example, the phase difference on the DVM ($\Delta\phi_{DVM}$) during the asymmetric wing clipping treatment was calculated as:

$$\Delta\phi_{DVM} = \frac{t_{DVM,clipped} - t_{DVM,unclipped}}{\text{wingbeat period}}, \quad (1)$$

where t is the muscle activation time.

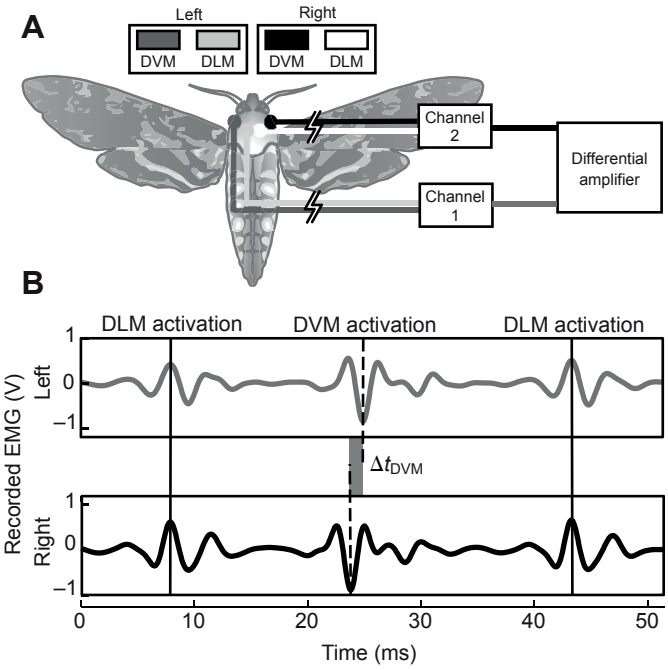

Fig. 2. Schematic diagram of electromyogram setup and activation phase extraction. (A) Ipsilateral electrodes implanted in four different muscles [left side dorsal ventral muscle (DVM) and dorsal longitudinal muscle (DLM), and right side DVM and DLM] connected to a differential amplifier. (B) Example of an activation phase extraction for the upstroke muscle (DVM), where Δt is the difference in activation time between the left and the right side or the unclipped and clipped side. To obtain the DVM phase difference ($\Delta\phi_{DVM}$) we divided Δt by the wingbeat period, which is the time between two subsequent DLM activation events (averaged between left and right sides).

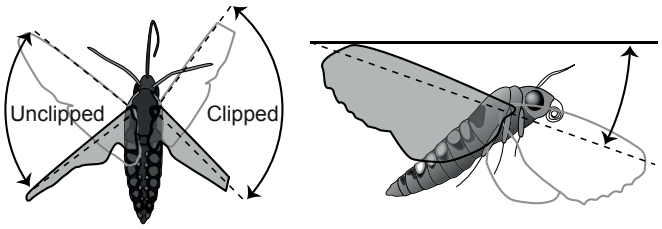

Fig. 3. Schematic diagram of the kinematic parameters. Although shown in overhead and lateral views, θ and β were calculated from the three-dimensional motion of the wing tip.

Flight kinematics and aerodynamic model

We recorded stable hovering flight using three high-speed video cameras (two Phantom v7.1 and one Phantom v5.1, Vision Research, Wayne, NJ, USA) at either 500 or 1000 frames s^{-1}. Wingbeat kinematic data were extracted from the videos through a 3-D kinematic reconstruction [DLTdv5 (Hedrick, 2008)]. We extracted wingbeat frequency (η), stroke amplitude (θ) and stroke plane angle (β) (see Fig. 3). Camera data were synchronized with EMG data by recording the camera activity signal with the data acquisition system.

With the above information (each moth's wing kinematics) and the morphology of each moth, we modelled the aerodynamic forces and torques produced by each flapping wing using a blade-element approach (Osborne, 1951; Sane, 2003; Weis-Fogh, 1973). In this approach, the lift on a flapping wing is given by:

$$F = \tfrac{1}{8}\rho\theta^2\eta^2 r_2 \overline{C_L}\overline{\left(\frac{d\hat{\theta}}{d\hat{t}}\right)^2}, \quad (2)$$

where ρ is air density, r_2 is the second moment of wing area, $\overline{C_L}$ is the whole-stroke average lift coefficient, and $\overline{(d\hat{\theta}/d\hat{t})^2}$ is the average square of the non-dimensional angular velocity of the wing. We used values of 1.66 for $\overline{C_L}$, following Willmott and Ellington's (Willmott and Ellington, 1997) results for hovering hawkmoths using a sinusoidal wing motion model and a $\overline{(d\hat{\theta}/d\hat{t})^2}$ of 19.74, characteristic of sinusoidal motion (Hedrick et al., 2009).

Using the same modelling framework, the magnitude of the aerodynamic torque from each flapping wing is given by:

$$\tau = \tfrac{1}{8}\rho\theta^2\eta^2 r_3 \overline{C_F}\overline{\left(\frac{d\hat{\theta}}{d\hat{t}}\right)^2}, \quad (3)$$

where r_3 is the third moment of wing area and $\overline{C_F}$ is the mean aerodynamic force coefficient for either lift or drag; $\overline{C_L}$ would give the predicted roll or pitch torque while $\overline{C_D}$, the coefficient of drag, yields the yaw torque magnitude. However, in this simple model of flapping flight, downstroke–upstroke, symmetries are expected to lead to zero net torque in pitch and yaw.

Statistical analysis

We investigated the effect of symmetric and asymmetric wing area reduction on muscle activity ($\Delta\phi_{DLM}$ and $\Delta\phi_{DVM}$) and wing kinematics (η, θ and β) using a linear mixed-effects model [nlme package of R 2.12 (Pinheiro et al., 2010; R Development Core Team, 2010)]. Time series of successive wingbeats were obtained from the same individual on different occasions (trials) as well as from different individuals (N=5). Conventional linear models (e.g. ANOVA) would not be the most appropriate statistical method because of the nested structure of the data (non-independence) and the unbalanced replication. We therefore used a three-level random intercepts model with sets of intercepts for the wingbeats in each trial (28 trials) for the trials of each treatment and for the treatments applied to each individual (Pinheiro and Bates, 2000). We checked for possible wingbeat autocorrelation because each trial consisted of many wingbeats. The autocorrelation function revealed a significant temporal autocorrelation that approximated a first-order auto-regressive [AR(1)] process. Consequently, an AR(1) correlation structure for the residuals was added to the best random intercepts model.

We chose the best model using Akaike's information criterion (AIC), an information-theoretic measure in which a model's log-likelihood penalized by the number of estimated parameters is used as a measure of fit (Burnham and Anderson, 2002). The best model among a set of candidate models is the one with the smallest AIC value. In the final model all the reported terms were judged statistically significant at α=0.05.

We also used linear and non-linear mixed-effect models and non-linear regression (MATLAB functions nlmefit and nlinfit) to examine the continuous relationship between the degree of wing asymmetry and muscle activation phase differences. For this portion of the study, we also conducted recordings on two additional moths with a smaller degree of wing reduction than was applied in the initial five moths used to test for differences among the control, asymmetric clipping and symmetric clipping treatments described above. Because wing asymmetry did not vary among the different wingbeats of a trial, we used mean values for the muscle activity and wing kinematic variables rather than a time series.

Table 2. Wingbeat kinematics [wingbeat frequency (η), stroke amplitude (θ), stroke amplitude difference (θ_{l-r}), stroke plane angle (β) and stroke plane angle difference between both wings (β_{l-r})] and neuromuscular activity ($\Delta\phi_{DLM}$ and $\Delta\phi_{DVM}$) during treatments (control, asymmetric wings and symmetric wings)

	Control	Asymmetric wings	Symmetric wings
η (Hz)	27.33±0.20	28.87±0.17	29.51±0.16
θ (deg) left wing	108.46±0.87	118.15±0.76	110.80±1.31
θ (deg) right wing	103.63±0.70	103.69±0.87	108.72±0.92
θ_{l-r} (deg)	2.20±0.80	14.46±0.95	1.25±0.87
β (deg) left wing	16.57±0.43	14.96±0.56	12.45±0.72
β (deg) right wing	17.59±0.39	17.65±0.56	12.64±0.92
β_{l-r} (deg)	0.06±0.30	–2.75±0.52	–0.90±0.16
$\Delta\phi_{DLM}$	0.0007±0.0007	0.0066±0.002	–0.0002±0.0008
$\Delta\phi_{DVM}$	0.02±0.003	0.05±0.003	0.01±0.003

Values were generated using all individuals (N=5) and all trials (N=28), excluding the additional moths with a smaller degree of wing reduction (N=2).
In the asymmetric wings column, the left wing corresponds to the clipped wing and the right wing corresponds to the unclipped wing, regardless of which wing was actually clipped. We calculated θ_{l-r}, β_{l-r}, $\Delta\phi_{DLM}$ and $\Delta\phi_{DVM}$ from the difference between clipped and unclipped wings.
Data are means ± s.e.m.
Data used in this table are available in supplementary material Table S2.

Table 3. Linear mixed-effect model table showing the effect of treatment on wingbeat kinematics (frequency, stroke amplitude and stroke plane angle) and neuromuscular activity (DLM and DVM phase differences)

	t	*P*
Frequency (η)		
Control *vs* asymmetric	4.934	<0.0001***
Control *vs* symmetric	6.150	<0.0001***
Asymmetric *vs* symmetric	0.681	0.078
Amplitude difference (θ_{l-r})		
Control *vs* asymmetric	5.987	<0.0001***
Control *vs* symmetric	0.973	0.343
Asymmetric *vs* symmetric	6.108	<0.0001***
Stroke plane angle difference (β_{l-r})		
Control *vs* asymmetric	2.184	0.040*
Control *vs* symmetric	0.655	0.519
Asymmetric *vs* symmetric	1.287	0.212
DLM phase difference ($\Delta\phi_{DLM}$)		
Control *vs* asymmetric	1.373	0.184
Control *vs* symmetric	0.161	0.873
Asymmetric *vs* symmetric	1.395	0.177
DVM phase difference ($\Delta\phi_{DVM}$)		
Control *vs* asymmetric	4.133	0.0005***
Control *vs* symmetric	1.877	0.0745
Asymmetric *vs* symmetric	5.579	<0.0001***

Trials nested in individuals are used as a random effect. We tested five moths, 28 trials and a total of 258 wingbeats (d.f.=21).
*P<0.05; ***P<0.001.
Data used in this table are available in supplementary material Table S2.

RESULTS

Overall mean and standard error values for wingbeat kinematics (absolute values for each wing: η, θ and β; differences between wings: $\Delta\theta_{l-r}$ and $\Delta\beta_{l-r}$) and neuromuscular activity ($\Delta\phi_{DLM}$ and $\Delta\phi_{DVM}$) are given in Table 2 for each experimental treatment.

We found that wingbeat frequency (η) increased following wing clipping. The linear mixed-effects model, with random effects based on trials nested within individuals, showed that wingbeat frequency was significantly different between the control and the experimental treatments (lme, P<0.0001; Table 3). However, the asymmetric treatment was not significantly different from the symmetrically clipped treatment (lme, P=0.078; Table 3, Fig. 4A).

When clipped asymmetrically, wing stroke amplitude (θ) increased on the clipped wing compared with the unclipped wing (Table 2). Therefore, $\Delta\theta_{l-r}$ showed a larger difference when wings were clipped asymmetrically compared with the control and symmetric clipping treatment (Fig. 4B). The linear mixed-effects model confirms this, showing that the asymmetric treatment was significantly different from the control and symmetric clipping treatments (lme, P<0.0001; Table 3), without showing a significant difference between control and the symmetric wing clipping (lme, P=0.343; Table 3).

Stroke plane angle (β) decreased in the clipped wing compared with the unclipped wing in the asymmetric treatment. Stroke plane angles for both wings were similar in the symmetrically clipped and control treatments. However, in the symmetric treatment, β of both wings decreased compared with the control treatment (Table 2). Among all three treatments, $\Delta\beta_{l-r}$ was only significantly different between the control and the asymmetric wing clipping treatment (lme, P=0.04; Table 3, Fig. 4C).

As described above, kinematic analysis of the asymmetric flight recordings showed that the damaged wing differed substantially from its pair. These changes were associated with a slight increase in $\Delta\phi_{DLM}$ and a large increase in $\Delta\phi_{DVM}$ in the clipped wing compared with the unclipped wing (Table 2). The $\Delta\phi_{DLM}$ results were not significantly different among treatments (lme, all P>0.18; Table 3, Fig. 3D) whereas the $\Delta\phi_{DVM}$ in the asymmetric treatment increased significantly compared with the control and symmetric treatments (lme, t=4.13, P=0.0005 and t=5.58, P<0.0001, respectively; Table 3,

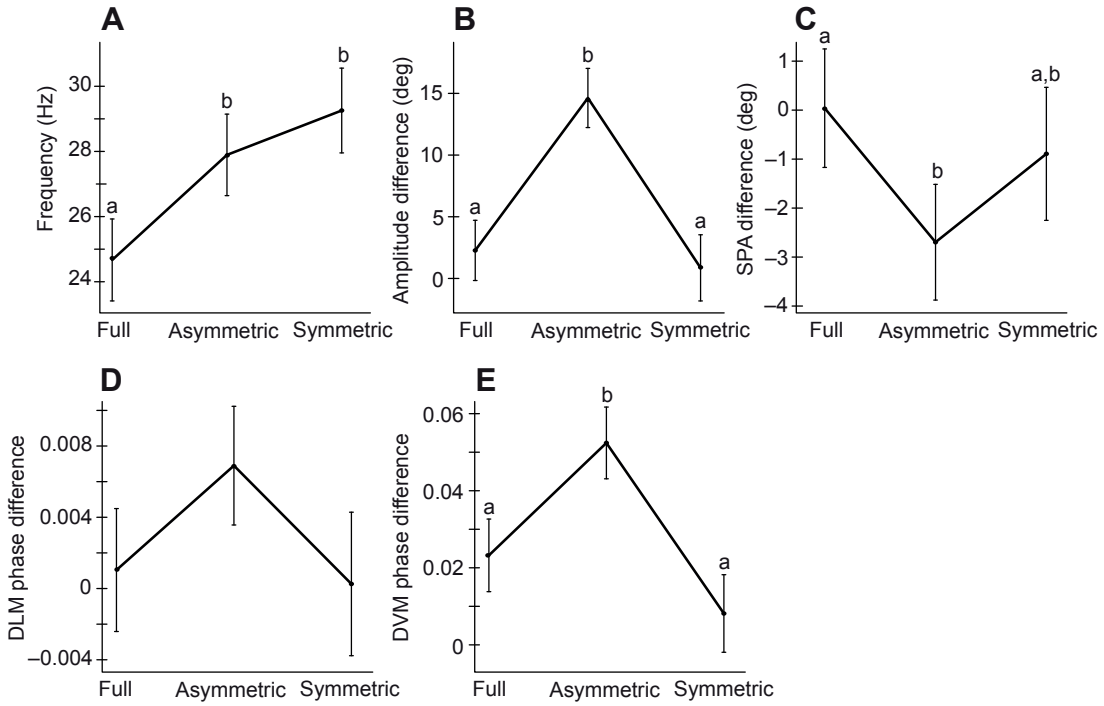

Fig. 4. Effect of experimental treatments (full, asymmetric and symmetric) on wingbeat kinematics and neuromuscular activity (linear mixed-effects model). (A) Wingbeat frequency (η). (B) Amplitude difference of both wings ($\Delta\theta_{l-r}$). (C) Stroke plane angle (SPA) difference of both wings ($\Delta\beta_{l-r}$). (D) DLM phase difference ($\Delta\phi_{DLM}$). (E) DVM phase difference ($\Delta\phi_{DVM}$). Data are means ± s.e.m. Different letters above the bars indicate significant differences between treatments.

Fig. 3E). During asymmetry, the upstroke muscle was delayed on the clipped wing compared with the unclipped wing. In the symmetric clipping treatment, activation timing differences returned to that observed in the control.

The blade-element aerodynamic model (Eqn 2) summed across both wings resulted in an estimated lift of 104.8±10.6% of body weight (mean±s.d.) for moths with intact wings, 102.9±9.3% for moths with asymmetrically clipped wings and 98.1±8.0% for moths with symmetrically clipped wings. These results are not significantly different from 100% of body weight, nor were any of the treatments significantly different from one another (one-way ANOVA, $F_{2,25}$=0.40, P=0.67). Furthermore, the blade-element model found no statistically significant lift asymmetries between the left and right or clipped and unclipped wings (Table 4); the observed asymmetries were not significantly different from zero (t-test, P>0.09 for all treatments). Blade-element torque predictions (Eqn 3) reveal a mean (±s.d.) asymmetry of 3.1±21.7% between the left and right wings of intact moths, a –22.3±7.8% asymmetry between the intact and clipped wings of asymmetrically clipped moths and a –1.4±18.8% torque asymmetry in symmetrically clipped moths. The torque asymmetry of the intact and symmetrically clipped moths was not significantly different than 0 (t-test, P>0.76 on both tests). However, the torque asymmetry predicted for the asymmetrically clipped moths was significantly greater than zero and significantly different from the other treatments (t-test, P=0.003; one-way ANOVA, $F_{2,25}$=5.98, P=0.007; all-pairs Tukey's HSD test, P<0.05), predicting less torque from the clipped wing in comparison to its pair.

Inspection of the relationship between muscle activation phase differences and morphological asymmetry revealed a strikingly non-linear relationship (Fig. 5), which we explored with a continuous non-linear model. We found that $\Delta\phi_{DVM}$ was best fit by the fractional difference in wing second moment of area raised to almost exactly the fourth power and the $\Delta\phi_{DVM}$ recorded in the control treatment for each moth (Fig. 5). In generating this model, we began with a linear mixed-effects model relating second moment of area and the $\Delta\phi_{DVM}$ recorded in the control to the $\Delta\phi_{DVM}$ observed in the asymmetric and symmetrically clipped treatments. We found that the magnitude of the moth random effects was less than 1/1000th the magnitude of the observations in models including $\Delta\phi_{DVM}$ control, thus we removed the random effect. We also noted the apparently non-linear relationship between second moment of area and $\Delta\phi_{DVM}$, and thus also fit a non-linear model with a higher-order polynomial relationship between the asymmetry in second moment of area and $\Delta\phi_{DVM}$. In both the linear and non-linear cases, we found that the 95% confidence interval for the intercept included zero; thus we dropped the intercept from both models. Finally, we compared the linear and non-linear models using an F-test; the non-linear model was found to be superior (P=0.0049), justifying inclusion of the non-linear polynomial term.

All measurement data are available in supplementary material Tables S1 and S2.

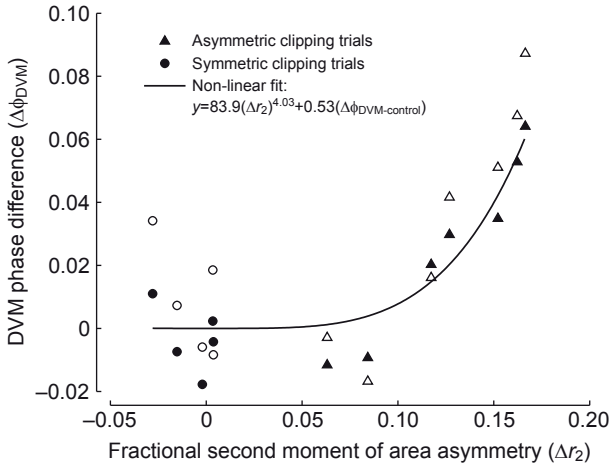

Fig. 5. The best supported model fitting mean DVM phase differences in symmetrically and asymmetrically clipped moths identified second moment asymmetry (normalized the difference in second moment of area among the wings divided by the second moment of area of the larger wing) raised to the ~4th power and the mean $\Delta\phi_{DVM}$ in the control treatment as significant factors. Here we show the fit of this model to the data for each moth in each treatment following adjustment for $\Delta\phi_{DVM\text{-}control}$. Note that this non-linear relationship predicts essentially no change in muscle activation timing at second moment asymmetries of <10%. Open symbols show the raw $\Delta\phi_{DVM}$ and filled symbols show $\Delta\phi_{DVM}$ adjusted for $\Delta\phi_{DVM\text{-}control}$.

DISCUSSION

We used measurements of flight muscle activity (bilateral DLM and DVM recordings) and wingbeat kinematics to investigate the mechanism used by *M. sexta* to compensate for asymmetric wing damage during free hovering flight. We hypothesized that moths would compensate for asymmetric wings *via* a passive mechanism based on muscle dynamics requiring minimal nervous intervention. Consequently, we expected to observe an increase in stroke amplitude on the damaged wing compared with the intact wing and an increase in the overall wingbeat frequency, but without corresponding asymmetries in the neural activation of the wing muscles.

Our kinematic findings generally match our predictions in that the damaged wing flapped with a larger amplitude than its undamaged counterpart. We also found an increase in wingbeat frequency following asymmetric or symmetric wing damage, similar to Sotavalta (Sotavalta, 1952). However, we did not find a significant further increase when we progressed from asymmetrically to symmetrically clipped wings, suggesting that total wing area alone does not predict changes in frequency.

Examining these results in the context of the blade-element force and torque model, we first found that the model performed adequately as a predictor of lift for untreated moths; modelled lift

Table 4. Total lift, lift asymmetry, net torque and torque asymmetry (mean ± s.e.m.) from the blade-element aerodynamic model under three treatments (full, asymmetric and symmetric)

Treatment	Total lift (N)	Lift asymmetry (%)	Net torque (Nm)	Torque asymmetry (%)
Full	0.0156± 0.01	6.5±6.4	0.00001±0.00006	3.1±21.7
Asymmetric	0.0155±0.01	–4.0±4.4	–0.00005±0.00002	–22.3±7.8*
Symmetric	0.0149±0.01	–0.9±8.7	–0.00001±0.00004	–1.4±18.8

*Significantly diffferent from the other treatments (P<0.05).
Data used in this table are available in supplementary material Table S1.

was not significantly different from body weight. This was also the case for both clipping treatments, where total lift from the two wings summed to equal body weight. The model also showed that the clipped and unclipped wings produced similar lift, i.e. the kinematic asymmetries exhibited by these moths were sufficient to restore symmetry in aerodynamic force production. However, this was not the case for aerodynamic torque, the modelled magnitude of which differed among the clipped and unclipped wings of asymmetric moths. This result does not match the predictions of our passive compensation model, which suggested that symmetric muscle activation should result in similar aerodynamic torques from asymmetric wings.

The results of our blade-element model indicate that moths with asymmetric wings do not produce identical (and thus offsetting) torques. In the case of yaw, this is not necessarily expected to lead to net rotational acceleration of the animal, as a blade-element flight model also predicts that each of the left and right wings produces a torque of equal magnitude and opposite direction during the downstroke and upstroke portions of the stroke cycle. For example, during downstroke the right wing produces a yaw torque to the right and during upstroke it produces a yaw torque to the left. Thus, left–right wing asymmetries will not necessarily produce a net yaw torque over a complete wingbeat cycle. The same principle applies to pitch torques, but this cannot be the case for lift-based roll torques because the direction of the torque from each wing is similar in downstroke and upstroke. Thus, based on the blade-element results described above, the hawkmoths should experience a net roll torque towards the clipped wing side. This is clearly not the case, as the animals maintained a stable orientation and did not exhibit any multi-stroke oscillations where the animal began to roll to one side over several wingbeats before applying a correction. Thus, factors not included in the blade-element model must explain the difference between the two results. These might include small shifts in the centre of mass location due to body rotation or a slight increase in the $\overline{C}_L$ of the clipped wing. Both of these effects may play a part. Due to wing twist, the distal portion of a wing has a reduced angle of attack compared with the proximal portion (Walker et al., 2009), possibly correlating with a lower local coefficient of lift. Clipping this portion may raise the whole wing $\overline{C}_L$ slightly. Furthermore, moths hovering with clipped wings appear to have a slight roll to the clipped side, which shifts the abdomen towards the unclipped wing, moving the centre of mass in that direction, reducing the torque asymmetry as applied to the whole animal but not to the muscles powering wing motion.

Our predictions, based on passive, mechanical compensation alone, require that moths compensate for wing asymmetries by changes in their kinematics without accompanying changes in neuromuscular modulation. However, contrary to these predictions, we found significant changes in the activation timing of the upstroke muscle (DVM). The DVM becomes active later in the stroke cycle on the damaged wing compared with the unclipped one. These muscle activation asymmetries are similar to observations from free flight yaw turns (Springthorpe et al., 2012; Wang et al., 2008). In these manoeuvres, the muscle on the side that the moth is turning towards becomes active earlier. Thus, our neuromuscular results are consistent with the moths continuously turning towards the undamaged wing side. Although moths with asymmetric wings and engaged in yaw turn manoeuvres exhibit a similar neural pattern, the muscle activation changes found in moths with asymmetric wings are much larger (~50 times greater for $\Delta\phi_{DVM}$) compared with the average results from voluntary yaw turns (phase differences of 0.05 and 0.001, respectively, for $\Delta\phi_{DVM}$; 0.006 and 0.003, respectively, for $\Delta\phi_{DLM}$) reported by Springthorpe et al. (Springthorpe et al., 2012). The asymmetrically clipped moths do have average activation phase differences that fall within the range exhibited by turning moths, which extends to 0.08 for $\Delta\phi_{DLM}$ and 0.07 for $\Delta\phi_{DVM}$.

Interestingly, when we clipped a smaller amount of the wing, between 4 and 7% of a single wing area, we still found a change in wing stroke amplitude (*t*-test, t=3.517, d.f.=3.41, P=0.032), but we found no asymmetry in the DVM muscle activation (*t*-test, t=–0.043, d.f.=7.989, P=0.966). This is reflected in the strongly non-linear relationship between morphological asymmetry as quantified by the second moment of wing area and DVM muscle activation asymmetry (Fig. 5), showing that asymmetries in the second moment of wing area of <10% require essentially no neural compensation, i.e. moths are able to compensate for small amounts of wing damage with minimal nervous intervention. Larger amounts of damage (>12% of second moment of wing area in this study) require active neuromuscular modulation to compensate for the larger perturbation. This use of active perturbation response in animals with substantial passive stability has also been shown in cockroaches that suffer large perturbations, in which case they cannot rely only on the mechanical feedback but require additional neural feedback to stabilize their locomotion (Sponberg and Full, 2008).

The apparent continuous manoeuvring required of the neuromuscular system of moths with asymmetric wings implies that such asymmetries may have a metabolic cost. Hedenström et al. (Hedenström et al., 2001) measured the metabolic cost during flight in bees with symmetrically clipped wings and found that wing clipping did not increase the metabolic costs during flight. This may relate to the symmetry of damage or its magnitude and location. In our case we applied damage at the wing tip, reducing area as well as the wing length and area moments, quantities important in lift and torque production. Hedenström et al. (Hedenström et al., 2001) applied damage along the trailing edge of the wing, leaving wing length unchanged and potentially changing the non-dimensional area moments less than our methods. This type of damage may require less compensation because of the smaller effect on wing aerodynamic function and the requirement for only a lift response rather than a lift and manoeuvring response, as is the case in asymmetric damage. Moreover, this study was performed with bees, which are asynchronous flyers and may need to modulate their individual wingbeats less compared with synchronous flyers such as moths. Further studies examining the cost of asymmetric wing clipping are therefore needed to examine a possible cost associated with a damage response based on continuous manoeuvring.

ACKNOWLEDGEMENTS

We wish to thank UNC's Integrative Mathematical Physiology discussion group for useful discussion, two anonymous referees for their feedback and Ellis Driver for contributions to the figure artwork.

FUNDING

This project was funded by the National Science Foundation (NSF IOS-0920358 to T.L.H.).

REFERENCES

Alcock, J. (1996). Male size and survival: the effects of male combat and bird predation in Dawson's burrowing bees, *Amegilla dawsoni*. *Ecol. Entomol.* **21**, 309-316.

Burnham, K. P. and Anderson, D. R. (2002). *Model Selection and Multimodel Inference*. New York: Springer-Verlag.

Büschges, A. (2005). Sensory control and organization of neural networks mediating coordination of multisegmental organs for locomotion. *J. Neurophysiol.* **93**, 1127-1135.

Cartar, R. V. (1992). Morphological senescence and longevity: an experiment relating wing wear and life span in foraging wild bumble bees. *J. Anim. Ecol.* **61**, 225-231.

Cheng, B., Deng, X. and Hedrick, T. L. (2011). The mechanics and control of pitching manoeuvres in a freely flying hawkmoth (*Manduca sexta*). *J. Exp. Biol.* **214**, 4092-4106.
Combes, S. A., Crall, J. D. and Mukherjee, S. (2010). Dynamics of animal movement in an ecological context: dragonfly wing damage reduces flight performance and predation success. *Biol. Lett.* **6**, 426-429.
Cruse, H. (1990). What mechanisms coordinate leg movement in walking arthropods? *Trends Neurosci.* **13**, 15-21.
Cruse, H., Dürr, V. and Schmitz, J. (2007). Insect walking is based on a decentralized architecture revealing a simple and robust controller. *Philos. Trans. R. Soc. Lond. A* **365**, 221-250.
Daley, M. A. and Biewener, A. A. (2006). Running over rough terrain reveals limb control for intrinsic stability. *Proc. Natl. Acad. Sci. USA* **103**, 15681-15686.
Daley, M. A., Voloshina, A. and Biewener, A. A. (2009). The role of intrinsic muscle mechanics in the neuromuscular control of stable running in the guinea fowl. *J. Physiol.* **587**, 2693-2707.
Dickinson, M. H., Farley, C. T., Full, R. J., Koehl, M. A. R., Kram, R. and Lehman, S. (2000). How animals move: an integrative view. *Science* **288**, 100-106.
Dietz, V., Quintern, J. and Sillem, M. (1987). Stumbling reactions in man: significance of proprioceptive and pre-programmed mechanisms. *J. Physiol.* **386**, 149-163.
Foster, D. J. and Cartar, R. V. (2011a). What causes wing wear in foraging bumble bees? *J. Exp. Biol.* **214**, 1896-1901.
Foster, D. J. and Cartar, R. V. (2011b). Wing wear affects wing use and choice of floral density in foraging bumble bees. *Behav. Ecol.* **22**, 52-59.
Gorassini, M. A., Prochazka, A., Hiebert, G. W. and Gauthier, M. J. A. (1994). Corrective responses to loss of ground support during walking. I. Intact cats. *J. Neurophysiol.* **71**, 603-610.
Haas, C. A. and Cartar, R. V. (2008). Robust flight performance of bumble bees with artificially induced wing wear. *Can. J. Zool.* **86**, 668-675.
Hedenström, A., Ellington, C. P. and Wolf, T. J. (2001). Wing wear, aerodynamics and flight energetics in bumblebees (*Bombus terrestris*): an experimental study. *Funct. Ecol.* **15**, 417-422.
Hedrick, T. L. (2008). Software techniques for two- and three-dimensional kinematic measurements of biological and biomimetic systems. *Bioinspir. Biomim.* **3**, 034001.
Hedrick, T. L., Cheng, B. and Deng, X. (2009). Wingbeat time and the scaling of passive rotational damping in flapping flight. *Science* **324**, 252-255.
Higginson, A. D. and Barnard, C. J. (2004). Accumulating wing damage affects foraging decisions in honeybees (*Apis mellifera* L.). *Ecol. Entomol.* **29**, 52-59.
Higginson, A. D. and Gilbert, F. (2004). Paying for nectar with wingbeats: a new model of honeybee foraging. *Proc. Biol. Sci.* **271**, 2595-2603.
Jindrich, D. L. and Full, R. J. (2002). Dynamic stabilization of rapid hexapedal locomotion. *J. Exp. Biol.* **205**, 2803-2823.
Kammer, A. E. (1971). The motor output during turning flight in a hawkmoth, *Manduca sexta*. *J. Insect Physiol.* **17**, 1073-1086.
Kingsolver, J. G. (1999). Experimental analyses of wing size, flight and survival in the western white butterfly. *Evolution* **53**, 1479-1490.
Marigold, D. S. and Patla, A. E. (2005). Adapting locomotion to different surface compliances: neuromuscular responses and changes in movement dynamics. *J. Neurophysiol.* **94**, 1733-1750.
McLachlan, A. J. (1997). Size or symmetry: an experiment to determine which of the two accounts for mating success in male midges. *Ecoscience* **4**, 454-459.
Nishikawa, K., Biewener, A. A., Aerts, P., Ahn, A. N., Chiel, H. J., Daley, M. A., Daniel, T. L., Full, R. J., Hale, M. E., Hedrick, T. L. et al. (2007). Neuromechanics: an integrative approach for understanding motor control. *Integr. Comp. Biol.* **47**, 16-54.
Osborne, M. F. M. (1951). Aerodynamics of flapping flight with application to insects. *J. Exp. Biol.* **28**, 221-245.
Pinheiro, J. C. and Bates, D. M. (2000). *Mixed-Effects Models in S and S-Plus*. New York: Springer-Verlag.
Pinheiro, J. C., Bates, D. M., DebRoy, S., Sarkar, D. and the R Development Core Team (2010). nlme: linear and nonlinear mixed effects models. R package version 3.1-97.
Pringle, J. W. S. (1957). *Insect Flight*. London: Cambridge University Press.
R Development Core Team (2010). R: A language and environment for statistical computing. Vienna: R Foundation for Statistical Computing. http://www.R-project.org/.
Revzen, S. (2009). Neuromechanical control architectures of arthropod locomotion. PhD dissertation, Department of Integrative Biology, University of California, Berkeley.
Rheuben, M. B. and Kammer, A. E. (1987). Structure and innervation of the third axillary muscle of *Manduca* relative to its role in turning flight. *J. Exp. Biol.* **131**, 373-402.
Ristroph, L., Bergou, A. J., Ristroph, G., Coumes, K., Berman, G. J., Guckenheimer, J., Wang, Z. J. and Cohen, I. (2010). Discovering the flight autostabilizer of fruit flies by inducing aerial stumbles. *Proc. Natl. Acad. Sci. USA* **107**, 4820-4824.
Robbins, R. K. (1981). The 'false head' hypothesis: predation and wing pattern variation of lycaenid butterflies. *Am. Nat.* **118**, 770-775.
Rodd, F. H., Plowright, R. C. and Owen, R. E. (1980). Mortality rates of adult bumble bee workers (Hymenoptera: Apidae). *Can. J. Zool.* **58**, 1718-1721.
Sane, S. P. (2003). The aerodynamics of insect flight. *J. Exp. Biol.* **206**, 4191-4208.
Sotavalta, O. (1952). The essential factor regulating the wing-stroke frequency of insects in wing mutilation and loading experiments and in experiments at subatmospheric pressure. *Ann. Zool. Soc. Vanamo* **15**, 1-67.
Sponberg, S. and Daniel, T. L. (2012). Abdicating power for control: a precision timing strategy to modulate function of flight power muscles. *Proc. R. Soc. Lond. B.* **279**, 3958-3966.
Sponberg, S. and Full, R. J. (2008). Neuromechanical response of musculo-skeletal structures in cockroaches during rapid running on rough terrain. *J. Exp. Biol.* **211**, 433-446.
Springthorpe, D., Fernández, M. J. and Hedrick, T. L. (2012). Neuromuscular control of free-flight yaw turns in the hawkmoth *Manduca sexta*. *J. Exp. Biol.* **215**, 1766-1774.
Swaddle, J. P. (1997). Within-individual changes in developmental stability affect flight performance. *Behav. Ecol.* **8**, 601-604.
Swaddle, J. P. and Witter, M. S. (1998). Cluttered habitats reduce wing asymmetry and increase flight performance in European starlings. *Behav. Ecol. Sociobiol.* **42**, 281-287.
Walker, S. M., Thomas, A. L. R. and Taylor, G. K. (2009). Photogrammetric reconstruction of high-resolution surface topographies and deformable wing kinematics of tethered locusts and free-flying hoverflies. *J. R. Soc. Interface* **6**, 351-366.
Wang, H., Ando, N. and Kanzaki, R. (2008). Active control of free flight manoeuvres in a hawkmoth, *Agrius convolvuli*. *J. Exp. Biol.* **211**, 423-432.
Weis-Fogh, T. (1973). Quick estimates of flight fitness in hovering animals, including novel mechanisms for lift production. *J. Exp. Biol.* **59**, 169-230.
Willmott, A. P. and Ellington, C. P. (1997). The mechanics of flight in the hawkmoth *Manduca sexta*. II. Aerodynamic consequences of kinematic and morphological variation. *J. Exp. Biol.* **200**, 2723-2745.
Wootton, R. J. (1992). Functional morphology of insect wings. *Annu. Rev. Entomol.* **37**, 113-140.